Journal of Inflammation Research

Dovepress
Taylor & Francis Group

Open Access Full Text Article

ORIGINAL RESEARCH

Dual Effects of Sodium Houttuyfonate Against Acute Rhinosinusitis: Antibacterial Action and Epithelial Barrier Repair Through the p38 MAPK/ERK Pathway

Yang Fang, Huixia Zhou, WeiYi Li, Lu Bai, Xinchen Sun, KaiYuan He, Shanshan Xue, Yongjun Wu

Department of Otolaryngology, Affiliated Hospital of Nanjing University of Chinese Medicine, Nanjing, Jiangsu, 210029, People's Republic of China

Correspondence: Shanshan Xue; Yongjun Wu, Email 390429607@qq.com; wooyongjun@126.com

Background: *Houttuynia cordata* Thunb, a traditional medicinal herb, is the source of sodium houttuyfonate (SH), a stabilized derivative with antibacterial, antiviral, and anti-inflammatory activities. Acute rhinosinusitis (ARS) comprises viral, post-viral, and bacterial forms; bacterial ARS causes severe inflammation and epithelial barrier disruption. Despite wide clinical use, the mechanisms of SH in ARS remain unclear.

Methods: Network pharmacology was applied to identify SH-associated targets and pathways. An ARS rat model was induced by inserting Staphylococcus aureus–soaked Merocel sponges into the nasal cavity. Rats received low, medium, or high doses of SH, with control and positive drug groups. Symptom scoring, CT, histopathology, hematology, ELISA, qRT-PCR, and immunohistochemistry were conducted. In vitro, human nasal epithelial cells (HNEpCs) were stimulated with lipopolysaccharide (LPS) and treated with SH, with or without MAPK modulators SB203580 (inhibitor) or Anisomycin (activator). Cell viability, cytokine expression, and ERK/p38 MAPK phosphorylation were assessed.

Results: SH improved nasal symptoms, reduced epithelial injury, and normalized nasal pH in ARS rats. It downregulated IL-1β, IL-6, TNF-α, and ICAM-1 while upregulating IL-4. Transmission electron microscopy showed restoration of ciliary and mitochondrial integrity. In HNEpCs, 60 μM SH was optimal by CCK-8 assay. In LPS-stimulated cells, SH suppressed IL-1β/IL-6 mRNA and inhibited ERK and p38 MAPK phosphorylation; these effects were reversed by Anisomycin, confirming pathway involvement.

Conclusion: SH alleviates sinonasal inflammation in ARS by inhibiting bacterial activity and restoring epithelial integrity through p38 MAPK/ERK suppression. These findings support SH as a potential therapy for upper airway inflammatory diseases.

Keywords: sodium houttuyfonate, acute rhinosinusitis, houttuynia cordata, p38 MAPK/ERK signaling, inflammation, ethnopharmacology

Introduction

Houttuynia cordata, a traditional Chinese medicinal herb that is also consumed as an edible vegetable, has been widely employed for managing upper respiratory infections. Sodium houttuyfonate (SH), a stable derivative of the plant's volatile component houttuynin, has demonstrated antibacterial, antiviral, and anti-inflammatory activities.[1,2] Clinically, SH is widely used as a natural antimicrobial agent to treat upper respiratory infections, including pharyngitis and bronchitis.[3–5] Despite its widespread clinical use, the mechanisms underlying the therapeutic effects of SH in ARS—particularly its regulation of inflammation-related pathways—remain unclear.

Acute rhinosinusitis (ARS) is a common inflammatory condition of the nasal and paranasal mucosa. ARS can be classified into viral, post-viral, and bacterial subtypes. Viral infections account for the majority of cases, but bacterial ARS is often more severe, characterized by persistent infection, intense inflammatory responses, and disruption of the epithelial barrier. Clinically, ARS presents with nasal congestion, purulent discharge, facial pressure, and impaired

Received: 13 May 2025
Accepted: 20 September 2025
Published: 29 September 2025

Graphical Abstract

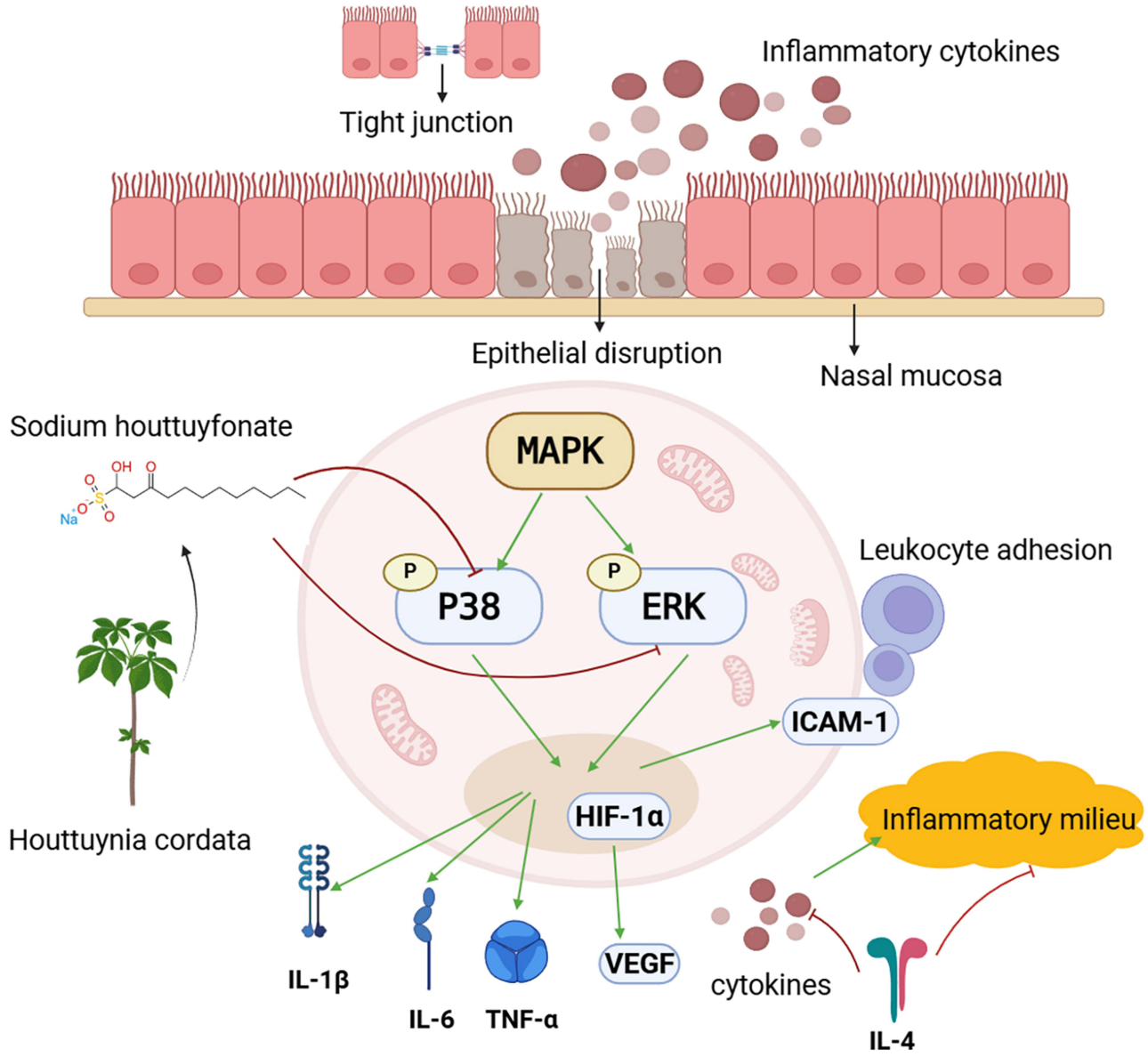

mucociliary clearance. While most viral or post-viral cases are self-limiting, bacterial ARS is prone to recurrent or chronic transformation, leading to reduced quality of patient survival and increased pressure on the healthcare system.[6,7] Epithelial damage and infiltration of inflammatory cells are central features of ARS pathophysiology.

Current treatments for ARS primarily involve symptomatic management, antibiotics, and corticosteroids. However, the overuse of antibiotics has raised concerns about antimicrobial resistance, and corticosteroids—though effective—may cause systemic side effects and are unsuitable for long-term use.[8,9] Therefore, there is a dire requirement to investigate alternative therapeutics that are both safer and more effective, particularly those capable of modulating mucosal inflammation and restoring epithelial integrity.

In this study, we explored the therapeutic mechanism of sodium houttuyfonate (SH) in acute rhinosinusitis (ARS) by integrating network pharmacology predictions with experimental validation. An ARS rat model was established by inserting sterile Merocel nasal sponges soaked in a *Staphylococcus aureus* suspension into the right nasal cavity. In

parallel, an in vitro epithelial inflammatory model was developed by stimulating human nasal epithelial cells (HNEpCs) with lipopolysaccharide (LPS). Particular attention was given to the MAPK signaling pathway, especially the p38 MAPK and ERK1/2 branches, which are known to regulate inflammatory cytokine production, epithelial barrier integrity, and mucosal immune responses.[10,11] Our objective was to determine whether SH ameliorates ARS by targeting MAPK signaling to suppress inflammation and protect epithelial structure and function.

Materials and Methods

To provide an overview of the study design, the integrated workflow is illustrated in Figure 1. Briefly, we first performed network pharmacology analysis to predict the potential targets and signaling pathways of sodium houttuyfonate (SH) against acute rhinosinusitis (ARS). Subsequently, the ARS rat model was established and treated with SH or reference drugs, followed by in vivo and in vitro validation experiments.

Network Pharmacology Prediction

The 2D molecular structure of sodium houttuyfonate (SH) was obtained using Marvin (https://freetrial.marvin.cxn.io/), and its potential target genes were predicted through the SwissTargetPrediction database (http://www.swisstargetprediction.ch/).[12] ARS-related genes were retrieved from GeneCards (https://www.genecards.org/), OMIM (https://www.omim.org/), and DrugBank (https://go.drugbank.com/) using the keyword "acute sinusitis" and limiting the species to "Homo sapiens". A network pharmacology approach was employed to identify the potential molecular targets of SH in the treatment of acute rhinosinusitis.[13] A Venn diagram was generated using the Bioinformatics platform (https://bioinformatics.com.cn/) to visualize the overlapping targets between SH and ARS. The intersecting genes were imported into the

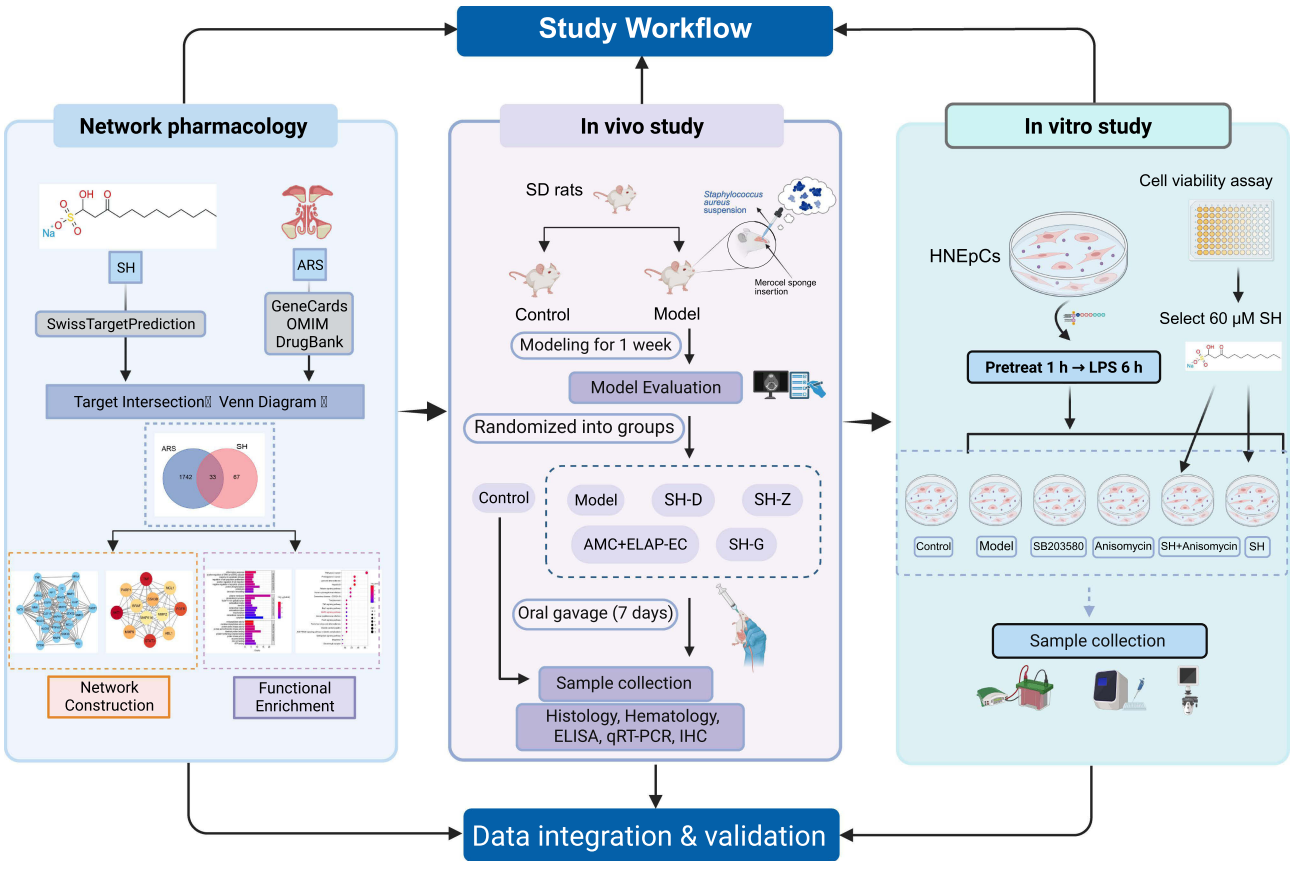

Figure 1 Overall workflow of the study. This workflow illustrates the integrated strategy for investigating sodium houttuyfonate (SH) against acute rhinosinusitis (ARS), combining network pharmacology prediction, in vivo animal experiments, and in vitro validation in HNEpCs to elucidate its therapeutic effects and underlying mechanisms. Created with BioRender.com.

STRING database (https://cn.string-db.org/) to construct a protein–protein interaction (PPI) network, applying a minimum required interaction score of 0.9 to ensure high-confidence associations. The resulting PPI network was visualized and analyzed using Cytoscape 3.10.2.[14] Gene Ontology (GO) and Kyoto Encyclopedia of Genes and Genomes (KEGG) enrichment analyses were performed using the DAVID database (https://david.ncifcrf.gov/) to explore the biological processes and pathways associated with the overlapping targets. The top 10 GO terms and top 20 KEGG pathways were selected based on p-value ranking and subsequently visualized via the Bioinformatics platform (http://www.bioinformatics.com.cn/) to highlight the key biological processes and signaling pathways involved in the pharmacological action of SH.

Experimental Validation of Predicted Targets

Animal-Based Evaluation of SH in ARS

Experimental Animals

60 SPF-grade male SD rats (6–8 weeks old, 230 ± 20 g) were obtained from Shanghai Bikai Keyi Biotechnology Co., Ltd. (license No. SCXK (Shanghai) 2023–0009). All animals were provided with irradiated and sterilized rodent feed formulated for growth and reproduction (Catalog No. XT101JX-001, purchased from Jiangsu Xietong Pharmaceutical Bio-engineering Co., Ltd). Rats were housed in a clean facility under controlled environmental conditions (temperature: 20–26 °C, relative humidity: 50–60%) and were acclimatized for 1 week before experimentation. All animal experiments were conducted in accordance with the Guide for the Care and Use of Laboratory Animals and were approved by the Laboratory Animal Ethics Committee of Nanjing University of Chinese Medicine (Approval No. 202310A040).

Main Reagents

Sodium houttuyfonate (SH, CAS No. 83766–73–8, purity ≥98%) was obtained from Shanghai Yuanye Biological Technology Co., Ltd. (Shanghai, China). Amoxicillin and Clavulanate Potassium Tablets (National Medicine Approval Number. H20053424), used as a positive control, were supplied by Lunan Better Pharmaceutical Co., Ltd. (Shandong, China). Eucalyptol, Limonene, and Pinene Enteric Capsules (National Medicine Approval Number. H20052401) were provided by Beijing Jiuhe Pharmaceutical Co., Ltd. (Beijing, China). Primary antibodies against TNF-α (Bioss, Catalog No. BS-10802R) and ICAM-1 (Proteintech, Catalog No. 16174-1-AP) were used for immunohistochemical analysis. A standard strain of *Staphylococcus aureus* (ATCC 6538) was obtained from Shanghai LuWei Biotechnology Co., Ltd. (China).

Establishment and Grouping of ARS Rat Models

After a one-week acclimatization period, 60 rats were randomly assigned to either the control group (n = 10) or the model group (n = 50). To induce acute rhinosinusitis (ARS), sterile Merocel nasal sponges were axially retained with microforceps and gently inserted into the right nasal passage of each anesthetized rat. Subsequently, 10 μL of *Staphylococcus aureus* suspension (1.2×10^9 CFU/mL) was instilled to saturate the sponge, thereby establishing localized infection and inflammation.[15] After one week, modeling success was evaluated based on behavioral symptom scoring for rhinosinusitis in rats. Animals with a total symptom score ≥ 6 and evidence of mucosal thickening or sinus fluid accumulation on CT imaging were considered successfully modeled for ARS.[16] Following model induction, five rats died during the procedure and were excluded from further analysis. The remaining 45 rats were randomly divided into five groups (n = 9 per group) for subsequent experiments: a model validation group, SH treatment groups: SH-D (low, 25 mg/kg), SH-Z (medium, 50 mg/kg), and SH-G (high, 100 mg/kg), and a positive drug control group. The positive control group received amoxicillin–clavulanate potassium tablets (AMC, 116 mg/kg) combined with eucalyptol-limonene-pinene enteric soft capsules (ELAP-EC, 92.5 mg/kg). The model validation group was administered deionized water (10 mL/kg/day) via oral gavage.

Observation Indicators

Observation of General Status and Cumulative Symptom Scores

The rats' mental status, behavior, physical appearance, food and water intake, as well as fecal and urinary characteristics were monitored daily. Particular attention was given to nasal symptoms, including the presence, amount, color, and

Table 1 Symptom Scoring Criteria for Acute Rhinosinusitis in Rats

Symptom	Mild (1 Point)	Moderate (2 Points)	Severe (3 Points)
Nose scratching (times)	1–4	5–9	≥10
Sneezing (counts)	1–4	5–9	≥10
Nasal discharge	Slight nasal discharge	Discharge flowing to nostrils	Discharge adhering around nasal area
Nasal inflammation	Nasal congestion	Nasal redness and swelling	Nasal swelling with bleeding

consistency of nasal discharge, mouth breathing (indicative of nasal obstruction), and nose-scratching behavior. Nasal symptoms were observed and recorded on days 1, 3, 5, and 7 after drug administration in each experimental group. Symptom severity was evaluated using a standardized scoring system for rhinosinusitis in rats (Table 1).

CT Imaging of the Paranasal Sinuses

High-resolution computed tomography (CT) was performed to assess sinus inflammation. Scans were acquired using a small-animal in vivo micro-CT imaging system (Quantum GX, USA). Rats were anesthetized prior to scanning, and images focused on the nasal and maxillary sinus regions. Mucosal thickening and the presence of sinus effusion were evaluated as indicators of inflammation severity across groups.

Measurement of Nasal Secretion PH

A precision pH test strip (Sanaisi, Shanghai, China; pH range: 6.4–8.0) was gently inserted into the right nasal cavity of rats using microforceps and held in place for 10 seconds. The pH value was then qualitatively assessed by the same investigator using a colorimetric reference chart.

Detection of Hematological

After 7 days of treatment, approximately 1–2 mL of blood was collected from the abdominal aorta of anesthetized rats for hematological analysis. The samples were gently inverted to mix with anticoagulant and left at room temperature for 10–15 minutes. White blood cells (WBC), neutrophils (NEU), lymphocytes (LYM) and monocytes (MONO) were counted and analyzed using a Mindray BC-30Vet fully automated veterinary blood analyzer (China). All samples were analyzed within 2 hours of collection to ensure data accuracy.

ELISA Analysis

Blood samples were collected from the abdominal aorta and centrifuged at 3000 rpm for 10 minutes at 4 °C to obtain serum. Serum concentrations of IL-1β (Catalog No. RX302869R), IL-6 (Catalog No. RX302870R), and IL-4 (Catalog No. RX302872R) were quantified using ELISA kits (RUIXIN, Fujian, China).

Immunohistochemistry of Sinonasal Mucosa Tissue

Sinonasal mucosal tissues were fixed in formalin, dehydrated, embedded in paraffin, and sectioned. Paraffin sections were subsequently deparaffinized and rehydrated, followed by antigen retrieval using microwave heating in citrate buffer (pH 6.0). To block endogenous peroxidase activity, the sections were treated with 3% hydrogen peroxide for 30 minutes and then incubated with 5% BSA to prevent nonspecific binding. Afterward, sections were incubated overnight at 4 °C with primary antibodies against TNF-α (1:1000) and ICAM-1 (1:1000). Following washing, HRP-conjugated secondary antibodies were applied for 30 minutes at room temperature. Signal visualization was performed using a DAB substrate kit, and nuclei were counterstained with hematoxylin. Images were captured under a light microscope, and positive staining areas were quantified using ImageJ software.

Histopathological Analysis of Sinonasal Mucosal Tissue

Sinonasal mucosal tissues were carefully collected, fixed in 4% paraformaldehyde, embedded in paraffin, and sectioned for histological analysis. Sections were stained with hematoxylin and eosin (H&E) to assess inflammatory changes. Additionally, small tissue fragments (~1 mm^3) were immersed in 2.5% glutaraldehyde for primary fixation, followed by

post-fixation in osmium tetroxide. After dehydration and resin embedding, ultrathin sections were prepared and examined under a transmission electron microscope (TEM) to evaluate ultrastructural alterations.

Quantification of mRNA Expression in Sinonasal Mucosa of ARS Rats

Approximately 30 mg of sinonasal mucosal tissue was retrieved from a –80 °C freezer and immediately homogenized in RNAex reagent (Catalog No. AG21101, Accurate Biology, China). Total RNA was extracted using the RNA Extraction Kit (Catalog No. AG21101-C, Accurate Biology, China), and its concentration and purity were assessed with a NanoDrop spectrophotometer (Thermo Fisher Scientific, USA). Subsequently, 1 μg of RNA from each sample was reverse-transcribed using the Reverse Transcription Kit (Catalog No. AG11728, Accurate Biology, China). Quantitative real-time PCR (qRT-PCR) was performed using the SYBR® Green Premix Pro Taq HS qPCR Kit (Catalog No. AG11718, Accurate Biology, China) on a QuantStudio™ 5 Real-Time PCR System (Thermo Fisher Scientific, USA). The relative expression of target genes was calculated using the $2^{-\Delta\Delta Ct}$ method, with GAPDH as the internal control. All primers were designed, synthesized, and purified by Sangon Biotech (Shanghai) Co., Ltd. (Table 2). The detailed experimental timeline of animal grouping, interventions, and sample collection is provided in Figure S1.

Cellular Mechanism Verification

Cell Culture

Human nasal epithelial cells (HNEPCs) were obtained from BeNa Culture Collection (BNCC, Catalog No. BNCC356247, China). Cell line identity was verified via short tandem repeat (STR) profiling. Cells were cultured in MEM supplemented with 10% fetal bovine serum (FBS) and 1% penicillin–streptomycin, and maintained at 37 °C in a humidified incubator with 5% CO_2.

Main Reagents

The CCK-8 kit (Biosharp, Catalog No. BS350B), MEM medium (BasaMedia, Catalog No. L550KJ), and fetal bovine serum (BDBIO, Catalog No. F801-500) were used for cell culture. Lipopolysaccharide (LPS, CAS No. 93572–42-0) was purchased from Sigma-Aldrich (St. Louis, MO, USA). SB203580 (CAS No. 152121–47-6) and Anisomycin (CAS No. 22862–76-6) were obtained from MedChemExpress (MCE, Monmouth Junction, NJ, USA). The following primary and secondary antibodies were used: phospho-p38 (Abcam, Catalog No. AB178867), p38 (Abcam, Catalog No. AB170099), phospho-ERK1/2 (Cell Signaling Technology, Catalog No. 4370), ERK1/2 (CST, Catalog No. 4695), β-Tubulin (Proteintech, Catalog No. 10068-1-AP), and goat anti-rabbit IgG (Immunoway, Catalog No. RS0002).

The Optimal Intervention Concentration of Sodium Houttuyfonate (SH) in LPS-Induced Injury of Human Nasal Epithelial Cells (HNEpCs) Was Evaluated Using a Cell Viability Assay (CCK-8)

HNEPC in the logarithmic growth phase was inoculated into 96-well plates at a density of 5000/well. After adherence, the complete medium was removed and replaced with serum-free basal medium for 12 hours to induce cellular starvation. SH was then administered at concentrations of 0, 15, 30, 60, 120, and 240 μM for 1 hour prior to LPS stimulation. Subsequently, lipopolysaccharide (LPS, 10 μg/mL) was added to induce an inflammatory response.[2] Each concentration was tested in triplicate. After incubation, the medium was discarded, and CCK-8 working solution was added to each well. Plates were

Table 2 Primer Sequences(Human)

Gene	Primer Sequences (5'→3')	bp
IL-6	F:AAGCCAGAGCTGTGCAGATGAGTA R: TGTCCTGCAGCCACTGGTTC	150
IL-1β	F: CCAGGGACAGGATATGGAGCA R: TTCAACACGCAGGACAGGTACAG	129
GAPDH	F: GCACCGTCAAGGCTGAGAAC R: TGGTGAAGACGCCAGTGGA	138

Table 3 Primer Sequences(Rat)

Gene	Primer Sequences (5'→3')	bp
p38MAPK	F: ACCTAAAGCCCAGCAACCTC R: AGCCCACGGACCAAATATCC	183
HIF-1α	F: CATCAAGTCAGCAACGTGGA R: GCACGTCATAGGCGGTTTCT	109
VEGF	F:CGGATCAAACCTCACCAAAGCC R:TTCTTTGGTCTGCATTCACATCTGC	80
GAPDH	F: GGCACAGTCAAGGCTGAGAATG R: ATGGTGGTGAAGACGCCAGTA	143

incubated for 1 hour, and absorbance was measured at 450 nm using a microplate reader. Cell viability was calculated using the following formula: $Viability\,(\%) = (A\_treatment - A\_blank)/(A\_control - A\_control\,blank) \times 100$

Cell Treatment

After 24 hours of adhesion culture, the medium was replaced with serum-free medium for 12 hours to induce nutrient starvation. Cells were then divided into six groups: Control, Model (LPS only), SH, SB203580, Anisomycin, and SH + Anisomycin. Except for the Control group, all cells were stimulated with LPS (10 μg/mL) for 6 hours to induce inflammation. Prior to LPS exposure, cells were pretreated for 1 hour with SH (60 μM) in the SH group, SB203580 (10 μM) in the SB203580 group, Anisomycin (10 μM) in the Anisomycin group, and both SH (60 μM) and Anisomycin (10 μM) in the SH + Anisomycin group. The Control group received no treatment.

Western Blot

HNEPC cells from each group were harvested and lysed using Western and IP cell lysis buffer, followed by lysis on ice for 30 minutes. Protein concentrations were determined using a BCA protein assay kit (Catalog No. P0012-1, Beyotime, Shanghai, China). SDS-PAGE separated equal amounts of total protein (30 μg per lane), transferred onto PVDF membranes, and blocked with 5% skim milk in TBST for 2 hours at room temperature. The membranes were then incubated overnight at 4 °C with primary antibodies against p38 (1:1000), phospho-p38 (1:1000), ERK1/2 (1:2000), and phospho-ERK1/2 (1:1000). Protein bands were visualized via enhanced chemiluminescence (ECL) and quantified with ImageJ software.

qRT-PCR

Total RNA was extracted from cultured cells using the same protocols and reagents as described above for tissue samples. Reverse transcription and quantitative real-time PCR were performed using the AG11728 and AG11718 kits (Accurate Biology, China), respectively. Relative gene expression levels were calculated using the $2^{-\Delta\Delta Ct}$ method, with GAPDH as the internal control. The primers used in the qRT-PCR assays were designed, synthesized, and purified by Sangon Biotech (Shanghai) Co., Ltd. (Table 3).

Statistical Analyses

Statistical analyses were conducted using GraphPad Prism software (version 8.0; GraphPad, USA). Data are presented as mean ± standard deviation (SD). Comparisons between two groups were made using an independent *t*-test (or a nonparametric test, where appropriate), while differences among multiple groups were evaluated by one-way ANOVA followed by Tukey's post hoc test. A p-value < 0.05 was considered statistically significant.

Result

Network Pharmacological Target Prediction

The two-dimensional molecular structure of SH is presented (Figure 2A). Using the GeneCards, OMIM, and DrugBank databases, a total of 1775 ARS-related target genes were collected (Figure 2B). Meanwhile, Based on

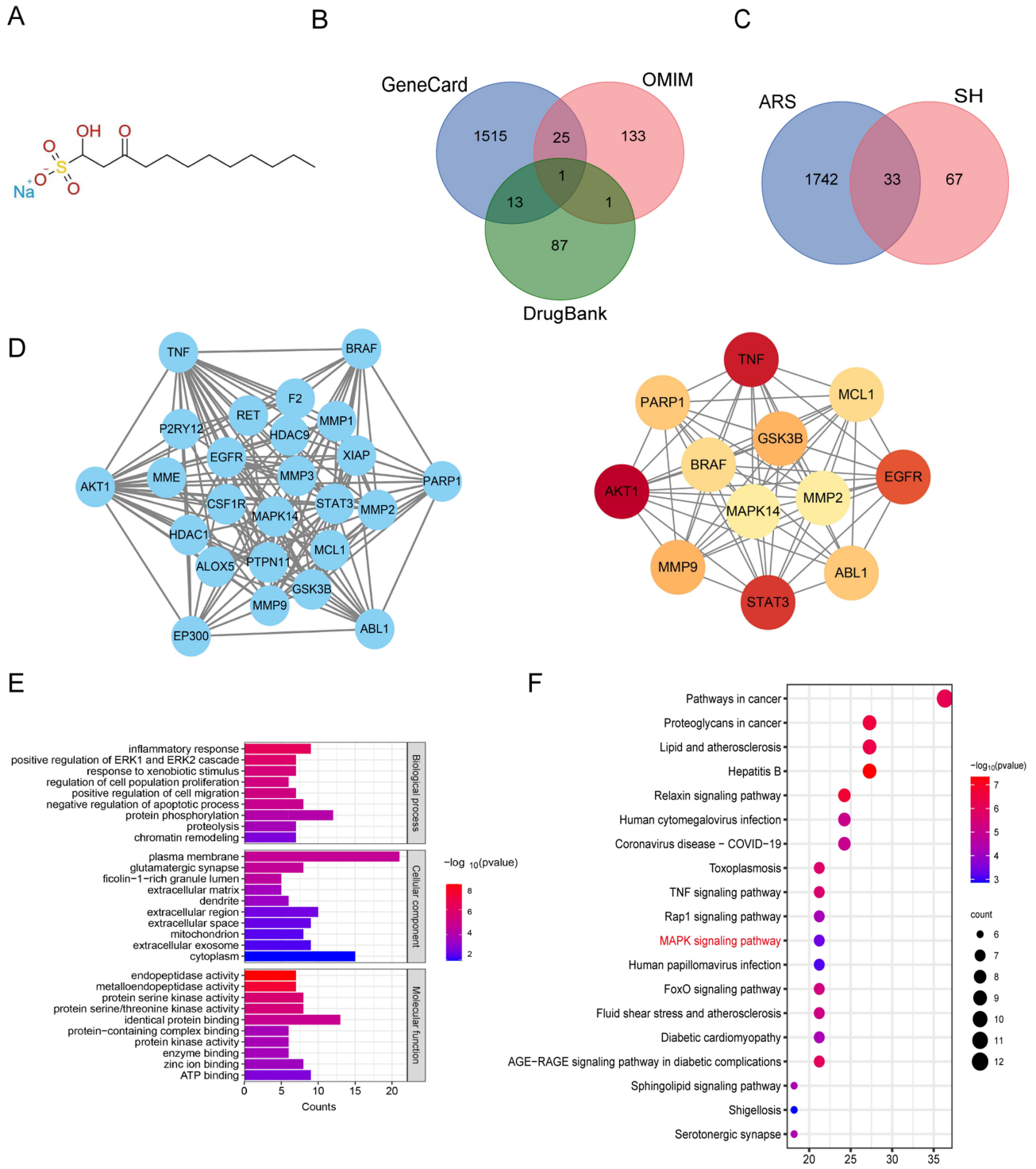

Figure 2 Network pharmacology analysis of SH against ARS. (**A**) 2D chemical structure of sodium houttuyfonate (SH). (**B**) Venn diagram of acute rhinosinusitis (ARS)-related targets from GeneCards, OMIM, and DrugBank databases. (**C**) Common targets of SH and ARS identified through Venn analysis. (**D**) Protein - protein interaction (PPI) network (left) and the top 12 hub genes (right) of the intersecting targets. In the right panel, node color ranges from red to yellow, indicating higher to lower degree values. (**E**) GO enrichment analysis, where distinct bar colors represent Biological Process (BP), Cellular Component (CC), and Molecular Function (MF). (**F**) KEGG pathway enrichment analysis. Bubble size represents the number of enriched genes, and color gradient from purple to red denotes enrichment significance (−log10 p value).

SwissTargetPrediction database, 100 SH targets were identified. A Venn diagram analysis revealed 33 overlapping genes shared between SH and ARS (Figure 2C). These intersecting genes were then input into the STRING database to construct a protein–protein interaction (PPI) network, consisting of 25 nodes and 149 edges (Figure 2D, left). The top 12 genes, including TNF, AKT1, STAT3, EGFR, MMP9, GSK3B, PARP1, ABL1, BRAF, MCL1, MMP2, and MAPK14 (p38), were identified based on degree ranking (Figure 2D, right). Gene Ontology (GO) enrichment analysis revealed that the key enriched biological processes include inflammatory response, positive regulation of ERK1 and ERK2 cascade, and response to xenobiotic stimulus, etc., and the main molecular functions are endopeptidase activity, metalloendopeptidase activity, protein serine kinase activity, etc (Figure 2E). KEGG pathway enrichment suggested that the therapeutic mechanism of SH against ARS may be associated with the TNF signaling pathway, Rap1 signaling pathway, and MAPK signaling pathway (Figure 2F). Based on these findings and previous literature, we hypothesized that SH may alleviate inflammatory responses by modulating the MAPK signaling pathway. Therefore, we selected the p38 MAPK/ERK pathway for in vivo and in vitro experimental validation.

In vivo Evaluation of SH in ARS Rats

Effects of SH on General Physical Condition

The ARS model was induced by inserting Merocel nasal sponges soaked with *Staphylococcus aureus* into the right nasal cavity. Seven days after nasal packing, model establishment was confirmed by clinical symptoms, CT imaging, nasal secretion pH, and representative histopathology (Figure 3A). CT imaging revealed mucosal thickening and/or fluid accumulation in the right sinus cavity (Figure 3B). In the model group, the right nasal cavity was filled with purulent secretions (Figure 3C). The pH of nasal secretions was measured, showing a significant decrease in the model group compared to the control group (Figure 3D). Histopathological analysis using HE staining demonstrated a disorganized arrangement of epithelial cells, with partial epithelial detachment and necrosis. Substantial inflammatory cell infiltration was observed in the sinonasal mucosal tissue of the model group (Figure 3E and F), whereas the control group exhibited normal histological architecture (Figure 3G and H).

Effects of SH on Nasal Symptoms

Macroscopic examination of the nasal cavities revealed that rats in the model group displayed prominent purulent discharge and crusting around the nostrils. In contrast, rats treated with SH (SH-D, SH-Z, SH-G) or the positive control (AMC + ELAP-EC) exhibited marked improvements in nasal appearance, with visibly reduced secretions and inflammation relative to the model group (Figure 4A).

Effects of SH on Paranasal Sinus CT Scans

CT imaging of the paranasal sinuses revealed mucosal thickening and fluid accumulation in the right sinus cavity of the model group, indicating pronounced sinus inflammation. In contrast, rats in the SH-treated groups and the AMC + ELAP-EC group showed reduced mucosal edema and clearer sinus cavities, suggesting that SH effectively alleviated sinus pathology (Figure 4B).

Effects of SH on Cumulative Symptom Scores

To comprehensively assess the impact of sinonasal mucosal inflammation and the therapeutic effect of SH, cumulative symptom scores were recorded on days 1, 3, 5, and 7 after treatment. The model group showed a progressive increase in cumulative scores over time. In contrast, all SH-treated groups and the positive control group demonstrated significantly lower symptom scores compared to the model group, in a time-dependent manner (Figure 4C).

Effects of SH on pH Value

A notable elevation in nasal pH was observed in the model group, suggesting disruption of mucosal homeostasis. SH treatment effectively normalized pH levels, with all SH-treated groups and the AMC + ELAP-EC group exhibiting marked improvements relative to the model group (Figure 4D).

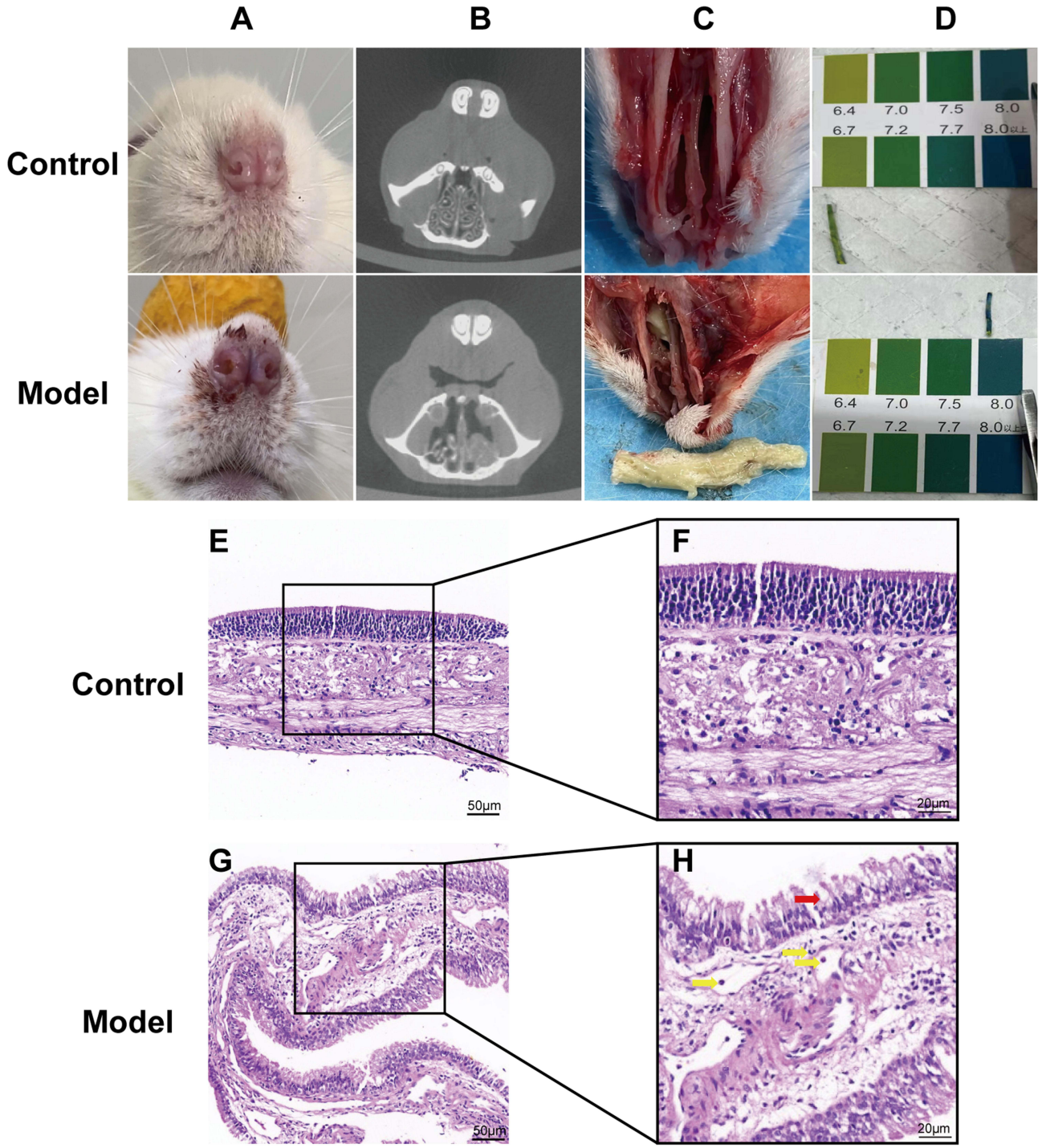

Figure 3 Validation of ARS rat model. (**A**) Nasal appearance of rats in control and model groups. (**B**) Coronal CT images showing mucosal thickening and effusion in the right sinus. (**C**) Gross morphology of sinonasal mucosa with purulent discharge in the model group. (**D**) Measurement of nasal secretion pH in control and model groups. (**E**–**H**) HE staining of sinonasal mucosa ((**E** and **F**): control; (**G** and **H**): model). Red arrows: ciliary loss; yellow arrows: mitochondrial swelling.

Effects of SH on Hematological Parameters

White blood cell (WBC), neutrophil (NEU), lymphocyte (LYM), and monocyte (MONO) counts were significantly higher in the model group than in the control group, indicating a systemic inflammatory response. SH treatment significantly reduced WBC, NEU, and MONO levels relative to the model group. Similar improvements were observed

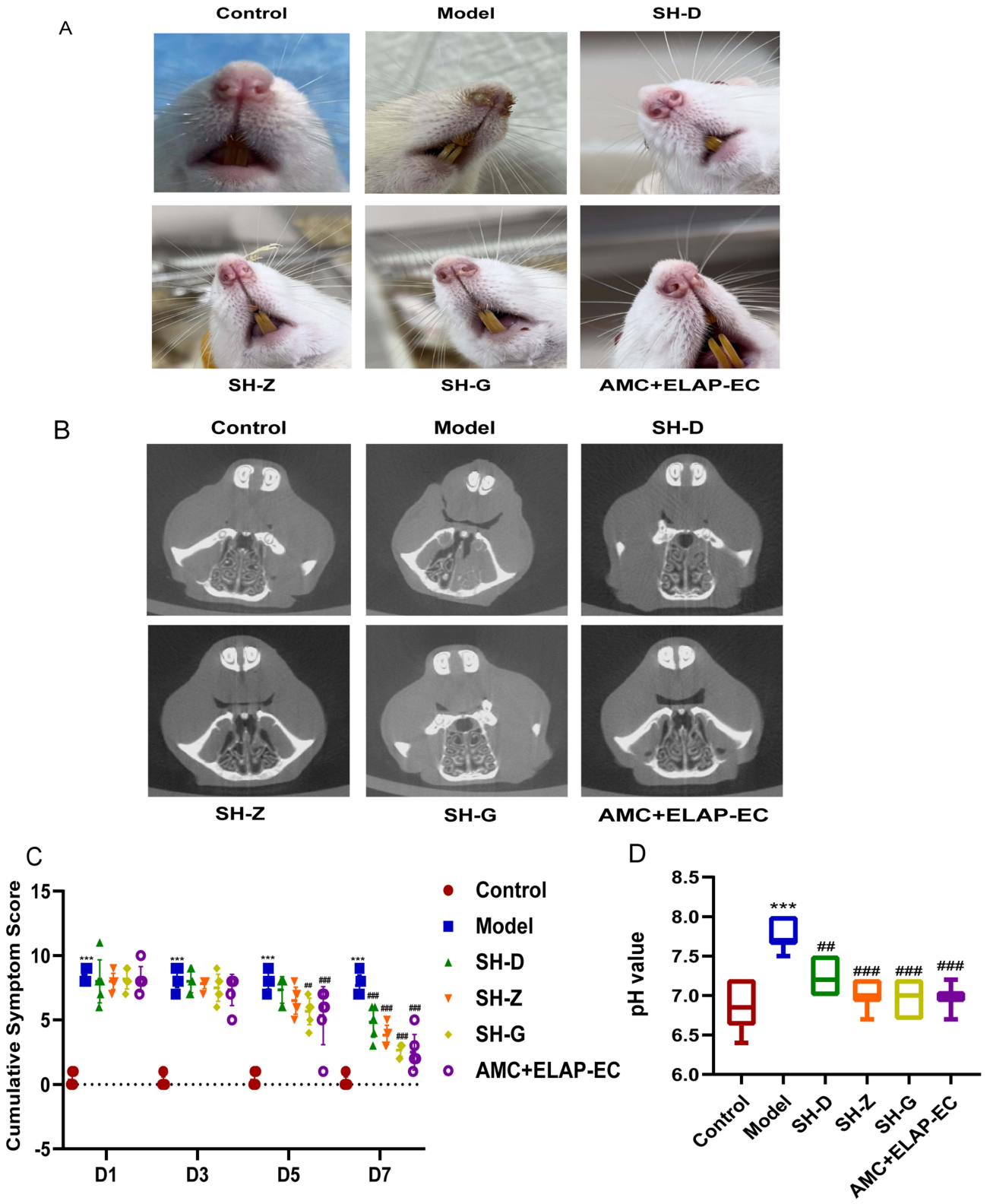

Figure 4 Therapeutic effects of SH on clinical symptoms and sinus pathology in ARS rats. (**A**) Representative nasal appearance in each group after 7 days of intervention. (**B**) CT scans showing sinus condition in each group. (**C**) Cumulative symptom scores on Days 1, 3, 5, and 7. (**D**) Nasal secretion pH values. (n = 6, ***p < 0.001 vs control, ##p < 0.01, ###p < 0.001 vs model).

https://doi.org/10.2147/JIR.S539966

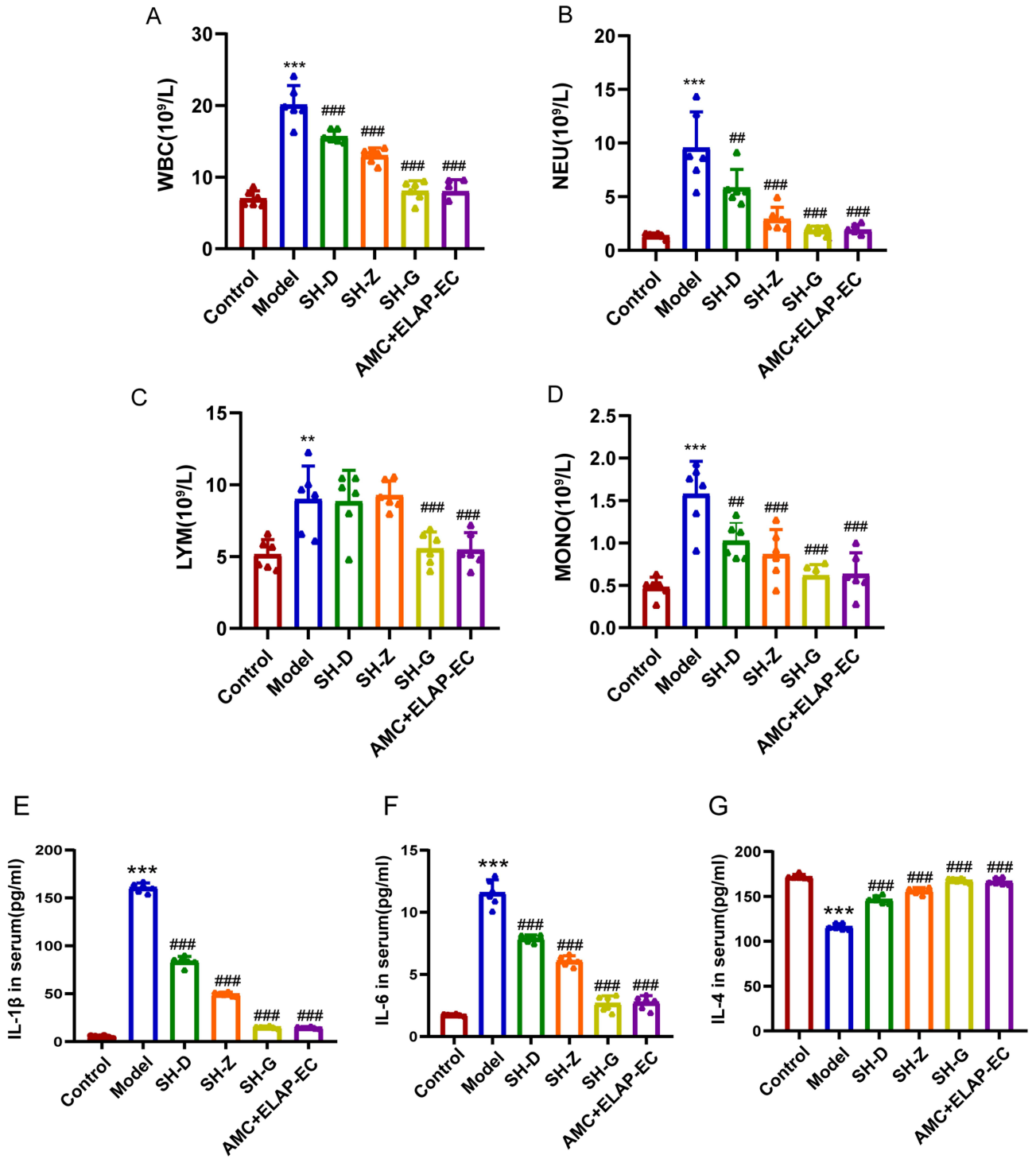

Figure 5 Effects of SH on blood cell counts and inflammatory cytokines in ARS rats. (**A**–**D**) WBC, NEU, LYM, and MONO counts. (**E**–**G**) Serum concentrations of IL-1β, IL-6, and IL-4 detected by ELISA. (n = 6, **p < 0.01, ***p < 0.001vs. control, ##p < 0.01, ###p < 0.001 vs model).

in the positive control group (AMC + ELAP-EC). Although LYM counts were slightly increased in the model group, treatment with SH or AMC + ELAP-EC brought them closer to baseline levels (Figure 5A–D).

Effects of SH on Inflammatory Cytokines

ELISA analysis revealed that serum levels of IL-1β and IL-6 were significantly elevated in the model group. Treatment with SH (all dose groups) and the positive control (AMC + ELAP-EC) significantly reduced the concentrations of both

cytokines, indicating effective suppression of the systemic inflammatory response (Figure 5E and 5F). Conversely, IL-4, an anti-inflammatory cytokine, was markedly decreased in the model group but significantly restored following SH or AMC + ELAP-EC treatment (Figure 5G).

Effects of SH on the Expression of TNF-α and ICAM-1 in Sinonasal Mucosa

To evaluate the anti-inflammatory effects of SH on sinonasal tissue, the expression levels of the inflammatory markers TNF-α and ICAM-1 were assessed (Figure 6A). Immunohistochemical staining revealed a marked increase in TNF-α and ICAM-1 expression in the sinonasal mucosa of ARS model rats compared to controls. In contrast, treatment with SH at all doses (SH-D, SH-Z, SH-G) and the positive control (AMC + ELAP-EC) significantly reduced both the intensity and positive area of TNF-α and ICAM-1 staining (Figure 6B and C).

Effects of SH on Sinonasal Mucosa Damage

To preliminarily assess the protective effects of SH in ARS rats, histopathological examinations were performed. Hematoxylin and eosin (HE) staining indicated that the model group exhibited epithelial disruption, inflammatory cell infiltration, edema, and partial epithelial shedding. These pathological changes were markedly alleviated in the SH-treated groups and the positive control group (AMC + ELAP-EC). Red arrows indicate epithelial damage and shedding; yellow arrows indicate areas of inflammatory infiltration (Figure 7A). Transmission electron microscopy (TEM) showed that control rats had intact ciliary structures and organelles. In contrast, the model group exhibited severe ultrastructural damage, including ciliary loss and swollen or degenerated mitochondria. SH and AMC + ELAP-EC treatment preserved epithelial ultrastructure. Red arrows indicate ciliary alterations; yellow arrows highlight mitochondrial swelling and inflammatory injury (Figure 7B).

Effects of SH on the mRNA Expression in Sinonasal Mucosa

Quantitative PCR analysis revealed that the mRNA expression levels of MAPK14, HIF-1α, and VEGF were markedly elevated in the model group relative to the control group (Figure 8A–C), suggesting activation of the MAPK and hypoxia-related pathways in acute rhinosinusitis. Treatment with SH at various doses (SH-D, SH-Z, SH-G) and with the positive control (AMC + ELAP-EC) significantly suppressed the upregulation of these genes, with the SH-G and AMC + ELAP-EC groups exhibiting the most pronounced inhibitory effects.

In vitro Validation in HNEpCs

CCK-8 Experiment to Detect the Optimal Concentration of SH

HNEpCs were stimulated with LPS (10 μg/mL) for 6 hours and subsequently treated with varying concentrations of SH (0, 15, 30, 60, 120, and 240 μM). The CCK-8 assay revealed a dose-dependent reduction in cell viability with increasing SH concentrations. The half-maximal inhibitory concentration (IC_{50}) of SH was calculated to be 68.91 μM. Following these findings, 60 μM was selected as the working concentration for subsequent in vitro experiments (Figure 9A).

Effect of SH on the Morphology Under Different Treatments

Brightfield microscopy revealed that HNEpCs in the model group exhibited morphological disruption, including cell shrinkage, detachment, and reduced cell density, whereas cells in the control group displayed an intact, polygonal shape with tight intercellular junctions. SH treatment markedly improved cell morphology, showing increased adherence and preserved cellular integrity. Similarly, treatment with the p38 MAPK inhibitor SB203580 yielded comparable protective effects. In contrast, the p38 MAPK agonist anisomycin reversed the beneficial effects of SH. Cells in the SH + anisomycin group exhibited partially preserved morphology compared to the model group, suggesting that SH may exert its cytoprotective effect via inhibition of the p38 MAPK pathway (Figure 9B).

Effects of SH on the MAPK Signaling Pathway in LPS-Damaged HNEpC Cells

Western blot examination showed that the model group had significantly higher levels of phosphorylated p38 (p-p38) and phosphorylated ERK (p-ERK) than the control group. SH treatment markedly reduced both p-p38 and p-ERK levels. Similarly, the p38 inhibitor SB203580 suppressed phosphorylation, whereas the p38 agonist Anisomycin significantly

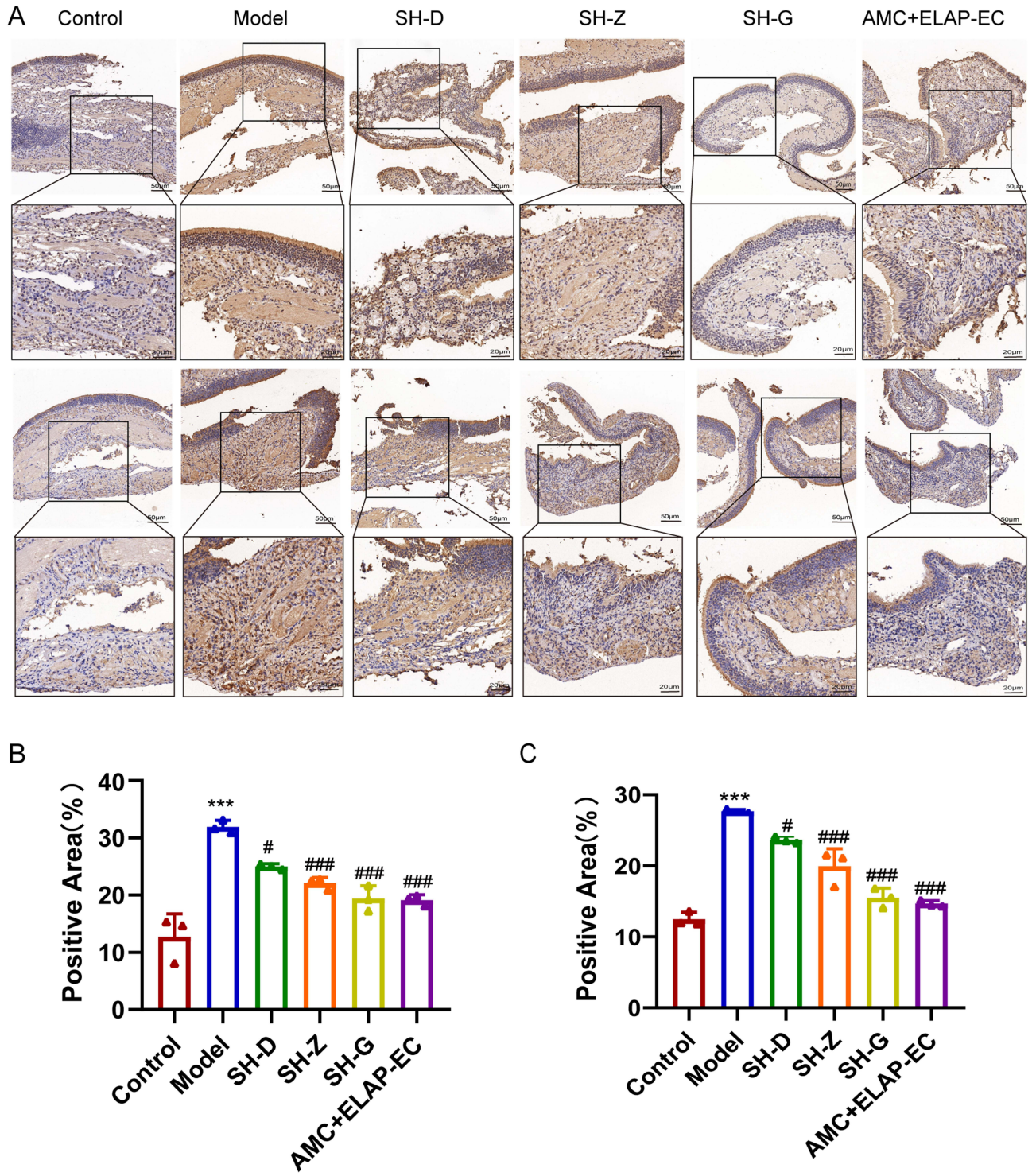

Figure 6 SH reduced inflammatory marker expression in ARS rat nasal mucosa. (**A**) Representative immunohistochemical staining of TNF-α (upper) and ICAM-1 (lower) in sinonasal mucosa across six groups (Control, Model, SH-D, SH-Z, SH-G, and AMC+ELAP-EC). (**B**) Quantification of TNF-α positive area (%). (**C**) Quantification of ICAM-1 positive area (%). *Data are presented as mean ± SD. (n = 3, ***p < 0.001 vs Control; #p < 0.05, ###p < 0.01 vs Model).

reversed the inhibitory effects of SH (Figure 10A). Quantitative analysis revealed a significant reduction in the p-p38/p38 and p-ERK/ERK ratios in both the SH and SB203580 groups, confirming the involvement of the p38 and ERK pathways (Figure 10B and C).

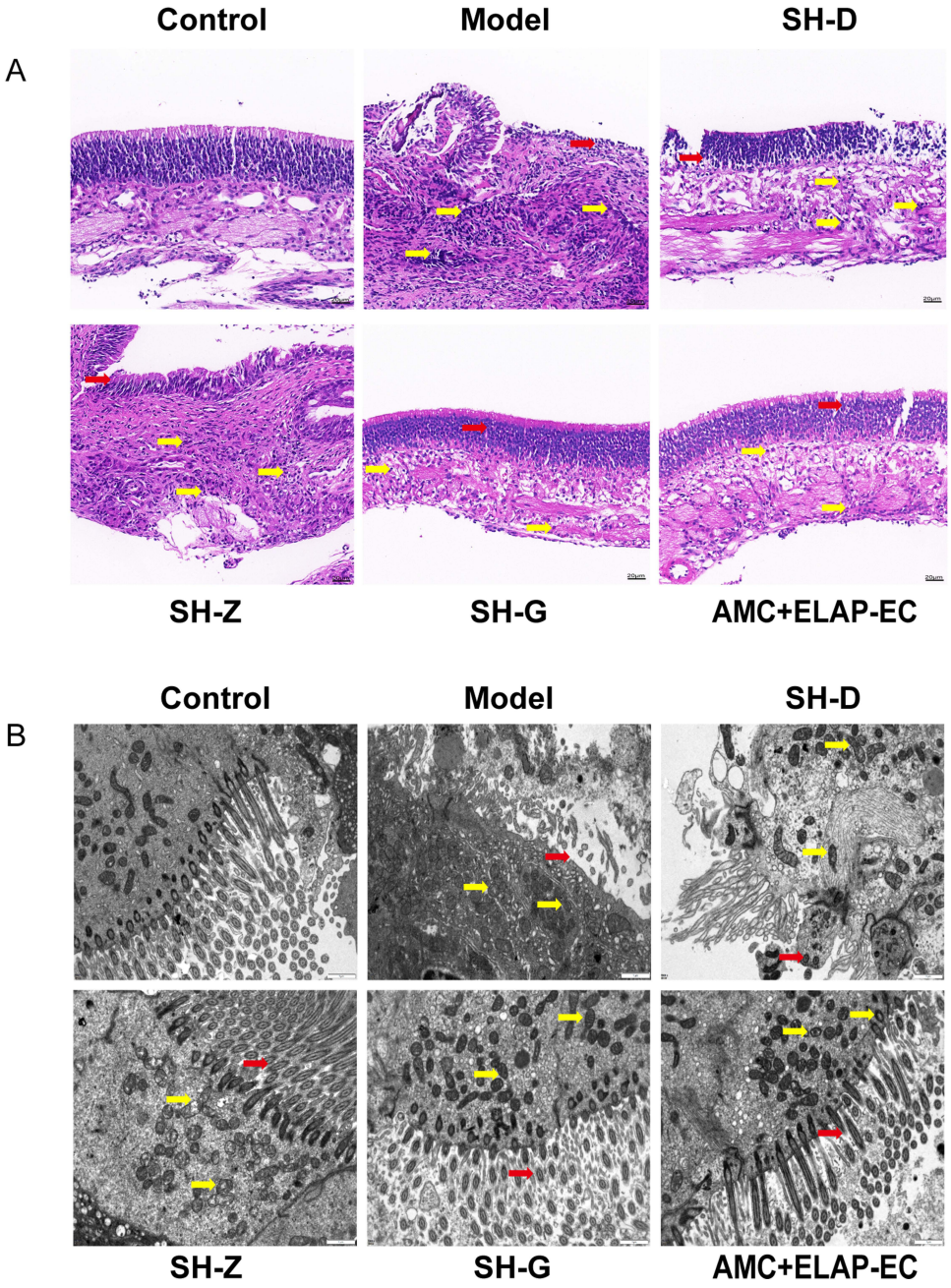

Figure 7 SH preserved sinonasal epithelial structure in ARS rats. (**A**) HE staining showing epithelial architecture and inflammatory infiltration. Red arrows indicate epithelial shedding; yellow arrows indicate inflammatory cell infiltration. (Scale bar = 20 μm). (**B**) TEM images showing ciliary structure and mitochondrial morphology in sinonasal mucosa. Red arrows indicate damaged cilia; yellow arrows indicate mitochondrial swelling. (Scale bar = 1 μm) Representative images from six groups are shown.

Effects of SH on the mRNA Expression of IL-1β and IL-6 in LPS-Stimulated Cells

qRT-PCR analysis revealed that the mRNA expression levels of IL-1β and IL-6 were significantly elevated in the model group. SH treatment markedly downregulated the expression of both cytokines. Similarly, SB203580 suppressed IL-1β and IL-6 expression, whereas Anisomycin treatment led to a pronounced increase. These findings suggest that SH mitigates inflammatory responses at least in part by inhibiting p38 MAPK activation (Figure 10D and E).

https://doi.org/10.2147/JIR.S539966

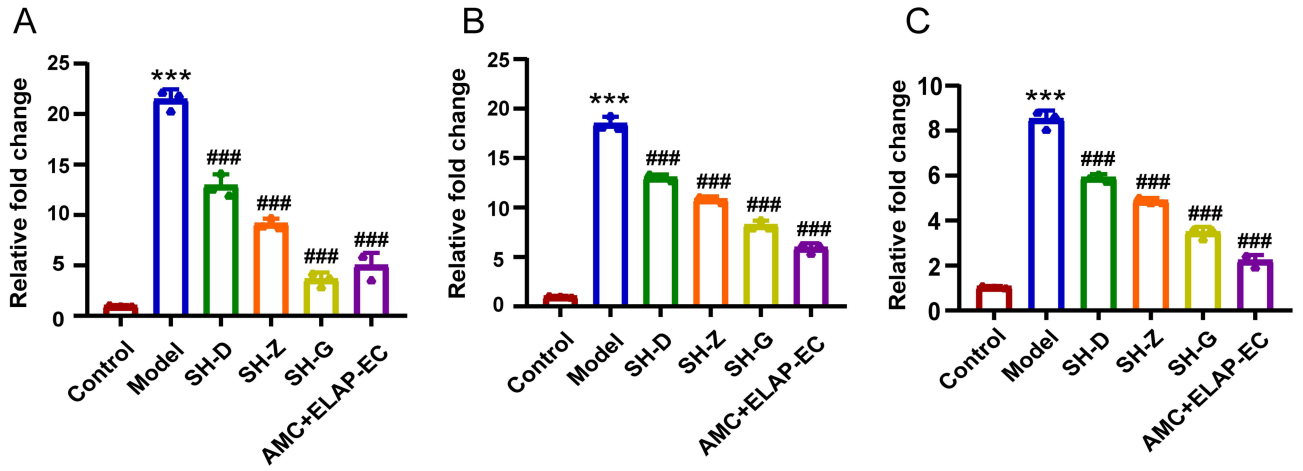

Figure 8 SH downregulates expression of inflammation- and hypoxia-related genes in ARS rats. (**A**–**C**) qRT-PCR results showing relative expression levels of MAPK14 (p38), HIF-1α, and VEGF. (n = 3, ***p < 0.001 vs control, ###p < 0.001 vs model).

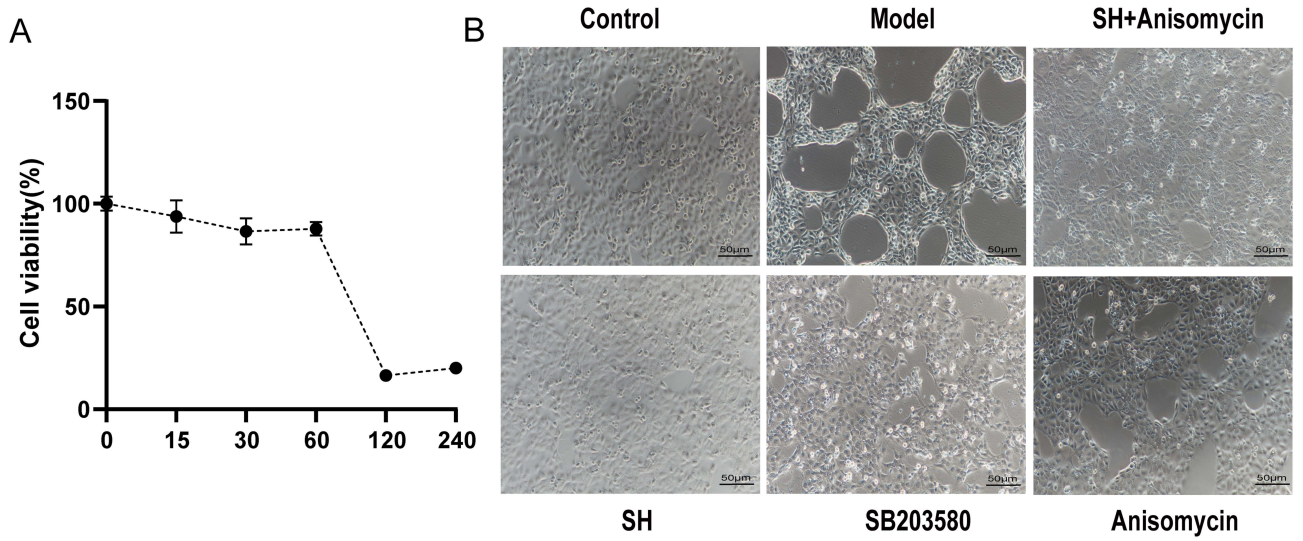

Figure 9 SH improves cell viability and morphology in LPS-induced Human Nasal Epithelial Cells injury model. (**A**) CCK-8 assay for optimal SH concentration. (**B**) Microscopy images showing morphology under various treatments (control, model, SH+Anisomycin, SH, SB203580, Anisomycin).

Discussion

It is commonly known that the MAPK signaling pathway plays a vital part in regulating key cellular processes, including morphogenesis, metabolism, and inflammation.[17] Recent studies have further implicated dysregulated MAPK activity in mucosal injury, ciliary dysfunction, and epithelial barrier disruption in upper respiratory tract disorders such as chronic rhinosinusitis with nasal polyps.[18] Sodium houttuyfonate (SH) is widely recognized for its anti-inflammatory and antimicrobial properties; however, its specific regulatory effects on MAPK signaling in acute rhinosinusitis (ARS) remain poorly understood. Elucidating this relationship is essential for understanding the pharmacological potential of SH and facilitating its clinical application.

This study combines network pharmacology with in vivo and in vitro experiments to investigate the therapeutic effects and potential mechanisms of SH in acute rhinosinusitis (ARS). SH treatment significantly alleviated nasal symptoms, normalized local pH, and improved radiological signs of sinus inflammation. Histopathological analysis confirmed reductions in epithelial damage, mucosal edema, and inflammatory cell infiltration. Systemic inflammatory indicators, including WBC, NEU, LYM, and MONO, were also decreased following SH administration. SH

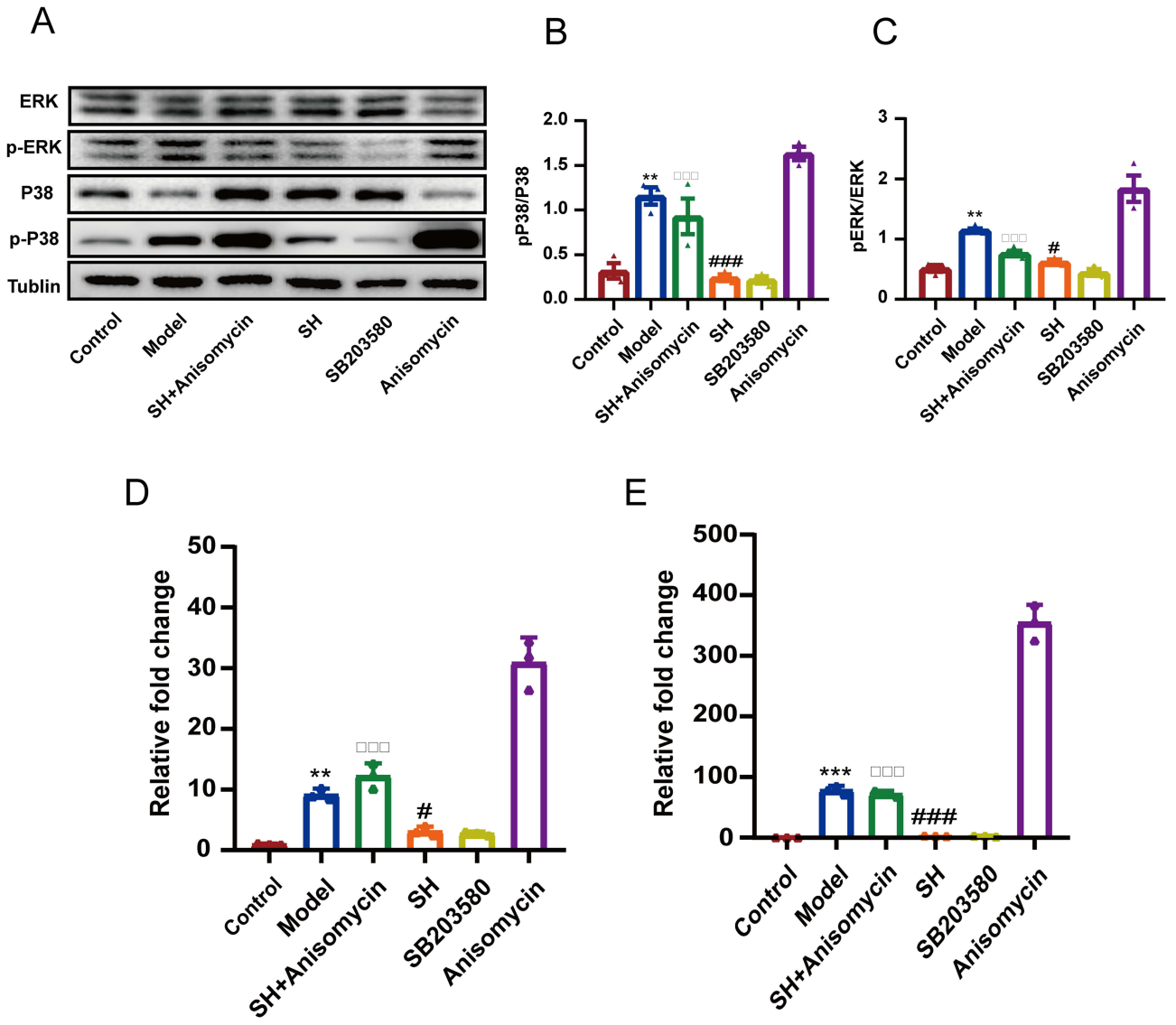

Figure 10 SH inhibits MAPK pathway activation and inflammatory gene expression in vitro. (**A**) Western blot bands showing p38, p-p38, ERK, p-ERK, and Tubulin expression. (**B** and **C**) Densitometric analysis of p-p38/p38 and p-ERK/ERK ratios. (**D** and **E**) qPCR analysis of IL-1β and IL-6 mRNA levels. (n = 3, **p < 0.01, ***p < 0.001 vs control, #p < 0.05, ###p < 0.001 vs model, □□□p < 0.001 vs Anisomycin).

downregulated proinflammatory cytokines (IL-1β, IL-6, TNF-α) while upregulating IL-4, a regulatory cytokine, suggesting both local and systemic immunomodulatory effects. These findings were consistent across both the ARS rat model and the LPS-induced HNEpC inflammation model, supporting SH's dual protective roles at the tissue and cellular levels.

In animal studies of acute rhinosinusitis (ARS), various modeling approaches have been reported. Traditional methods often involve surgical opening of the maxillary sinus followed by bacterial instillation into the sinus cavity.[19] While this approach may reliably induce localized inflammation, it does not adequately replicate the natural pathogenesis of ARS. Moreover, the surgical procedure compromises the anatomical integrity of the sinus cavity, disrupts capillary networks and ciliary structures, and introduces additional tissue injury and postoperative inflammation. In contrast, intranasal instillation of *Staphylococcus aureus* alone has been found to yield low infection rates.[20] Therefore, a model that more closely mimics the etiology and progression of human ARS, without introducing artificial injury, is crucial. In this study, we established an ARS rat model using expanding nasal sponges combined with intranasal instillation of *Staphylococcus aureus* suspension. This method, which closely mimics the dual pathogenic mechanisms of mechanical obstruction and bacterial infection seen in clinical ARS, avoids invasive surgical manipulation and preserves the integrity

https://doi.org/10.2147/JIR.S539966

of the sinonasal structures. Compared with maxillary sinus surgery-based approaches, this model more accurately reflects the natural progression of mucosal inflammation and has been shown to reduce procedural variability and epithelial damage unrelated to disease. The pathological features observed in our model—such as mucosal edema, epithelial disruption, and inflammatory infiltration—were similar to earlier investigations,[20,21] supporting the validity and reproducibility of this modeling strategy for therapeutic evaluation.

HE staining and transmission electron microscopy (TEM) provided further evidence of the mucosal protective effects of SH. In the model group, nasal epithelial disruption, ciliary loss, and mitochondrial swelling were consistently observed, accompanied by mucosal edema and inflammatory cell infiltration. These structural abnormalities impair mucociliary clearance and barrier function—two essential defense mechanisms of the upper respiratory tract.[22] Notably, SH treatment preserved epithelial integrity, mitigated ciliary damage, and restored mitochondrial morphology. Mitochondria are critical for supporting ciliary motion and epithelial regeneration, and their dysfunction may exacerbate local oxidative stress and inflammation.[23,24] Additionally, alterations in nasal pH observed in the ARS group reflected a disrupted epithelial microenvironment, while SH partially corrected this pH imbalance, suggesting improved barrier stability. In addition to structural damage, the pH of nasal secretions serves as a functional biomarker of mucosal microenvironmental stability. Under physiological conditions, the pH remains mildly acidic, supporting both mucociliary clearance and antimicrobial activity.[25] ARS model rats exhibited a significant shift toward alkalinity, consistent with epithelial injury and neutrophil activation. SH treatment partially restored pH levels toward normal, further supporting its role in maintaining mucosal homeostasis.

Mechanistically, our data suggest that SH exerts its anti-inflammatory effects by modulating the MAPK signaling pathway, particularly the p38 MAPK and ERK1/2 branches. These kinases regulate the expression of downstream proinflammatory mediators such as IL-1β, IL-6, and TNF-α, which play central roles in the inflammatory cascade of ARS. SH treatment significantly reduced the phosphorylation levels of p38 and ERK1/2 in both in vivo and in vitro models, confirming its inhibitory effect on this signaling axis. In the current investigation, we specifically concentrated on these two branches of the MAPK pathway due to their well-established involvement in inflammation and epithelial injury. Other MAPK components—especially JNK—were not included in the current investigation and warrant future exploration. Moreover, SH also downregulated ICAM-1, a key adhesion molecule that facilitates leukocyte infiltration and contributes to epithelial damage during acute inflammation.[26,27] This dual modulation of intracellular signaling and intercellular adhesion highlights SH's capacity to attenuate inflammation and preserve mucosal integrity on multiple levels.

Taken together, our findings not only provide experimental evidence that SH effectively alleviates ARS-related inflammation and epithelial damage, but also establish a mechanistic link between SH treatment and MAPK pathway modulation. Previous studies have investigated various anti-inflammatory therapies for ARS, including macrolide antibiotics, corticosteroids, and traditional herbal formulations. While antibiotics primarily reduce bacterial load and corticosteroids suppress local inflammation, both strategies are associated with adverse effects and limited long-term efficacy.[6,8] In contrast, SH exhibited broader pharmacological actions—not only suppressing proinflammatory cytokine expression but also preserving epithelial structure and restoring mucosal pH. This multifunctional activity underscores its therapeutic advantage over conventional interventions.

In addition to the MAPK pathway, several other signaling cascades may contribute to the pathogenesis of ARS and the pharmacological actions of SH. For instance, the NF-κB and TLR4 pathways are important regulators of innate immune responses and may operate prior to MAPK activation. Although these mechanisms were not experimentally investigated in the present study, they have been well documented in other models.[28] Moreover, SH was found to modulate the expression of HIF-1α and VEGF, indicating its potential involvement in hypoxia-mediated inflammation and vascular remodeling. Future studies should explore these additional pathways to gain a more comprehensive understanding of SH's anti-inflammatory mechanisms. Unlike conventional antibiotics or corticosteroids, SH exhibits the ability to simultaneously regulate cytokine expression, preserve epithelial architecture, and modulate intracellular signaling. These multifunctional properties highlight its therapeutic potential for ARS and other upper airway inflammatory diseases. Several limitations of this study should be acknowledged. First, all therapeutic effects were demonstrated in animal and cellular models; therefore, clinical studies are needed to confirm translational relevance. Second, although this work primarily focused on the MAPK signaling axis, other pathways—such as NF-κB and TLR4—may also contribute to the mechanisms of SH and should be

explored in future studies. Third, while SH is a defined derivative of Houttuynia cordata, its pharmacokinetic properties and long-term safety profile remain incompletely characterized and warrant further investigation. Fourth, bacterial ARS in our model was confirmed based on multiple complementary indicators, including clinical manifestations, hematological alterations, imaging evidence, and histopathological features. Nevertheless, we did not perform direct bacterial load quantification (eg, CFU counts), which remains a limitation of the present study. Future research should incorporate CFU or molecular quantification methods to further strengthen model validation.

Conclusion

Taken together, sodium houttuyfonate significantly attenuates sinonasal mucosal inflammation, improves epithelial integrity, and inhibits p38 MAPK and ERK1/2 signaling in both in vivo and in vitro ARS models. Collectively, these findings demonstrate the dual anti-inflammatory and mucosal-protective effects of SH and suggest its potential as a natural therapeutic agent for managing acute rhinosinusitis.

Abbreviations

ARS, Acute rhinosinusitis; AMC, amoxicillin–clavulanate potassium tablets; ELAP-EC, eucalyptol-limonene-pinene enteric soft capsules; HNEpC, human nasal epithelial cell; LPS, lipopolysaccharide; LYM, lymphocytes; MONO, monocytes; NEU, neutrophils; SH, sodium houttuyfonate; TEM, transmission electron microscope; WBC, White blood cells.

Acknowledgment

Graphical abstract is created in BioRender. yang, f. (2025) https://BioRender.com/b8juamq.

Author Contributions

All authors made a significant contribution to the work reported, whether that is in the conception, study design, execution, acquisition of data, analysis and interpretation, or in all these areas; took part in drafting, revising or critically reviewing the article; gave final approval of the version to be published; have agreed on the journal to which the article has been submitted; and agree to be accountable for all aspects of the work.

Funding

This research was funded by the National Natural Science Foundation of China (No.82174446).

Disclosure

The authors have declared that no competing interests exist in this work.

References

1. Wei PP, Luo Q, Hou Y, Zhao FL, Li F, Meng QG. *Houttuynia cordata* Thunb.: a comprehensive review of traditional applications, phytochemistry, pharmacology and safety. *Phytomedicine*. 2024;123:155195. doi:10.1016/j.phymed.2023.155195
2. Liu GX, Xiang H, Tang XD, et al. Transcriptional and functional analysis shows sodium houttuyfonate-mediated inhibition of autolysis in *Staphylococcus aureus*. *Molecules*. 2011;16(10):8848–8865. doi:10.3390/molecules16108848
3. Hu MX, Jin F, Zhang CC, et al. Sodium houttuyfonate induces bacterial lipopolysaccharide shedding to promote macrophage M1 polarization against acute bacterial lung infection. *Biomed Pharmacother*. 2024;179:117358. doi:10.1016/j.biopha.2024.117358
4. Shen YH, Cheng MH, Liu XY, Zhu DW, Gao J. Sodium houttuyfonate inhibits bleomycin-induced pulmonary fibrosis in mice. *Front Pharmacol*. 2021;12:596492. doi:10.3389/fphar.2021.596492
5. Wu Z, Deng XY, Hu QC, et al. Houttuynia cordata Thunb.: an ethnopharmacological review. *Front Pharmacol*. 2021;12:714694. doi:10.3389/fphar.2021.714694
6. Fokkens WJ, Lund VJ, Hopkins C, et al. European position paper on rhinosinusitis and nasal polyps 2020. *Rhinology*. 2020;58(Suppl 29):1–464. doi:10.4193/Rhin20.600
7. Bhattacharyya N. Contemporary incremental healthcare costs for chronic rhinosinusitis in the United States. *Laryngoscope*. 2021;131(10):2169–2172. doi:10.1002/lary.29454
8. Lemiengre MB, van Driel ML, Merenstein D, Liira H, Mäkelä M, De Sutter AIM. Antibiotics for acute rhinosinusitis in adults. *Cochrane Database Syst Rev*. 2018;9:CD006089. doi:10.1002/14651858.CD006089.pub5
9. Rosenfeld RM, Piccirillo JF, Chandrasekhar SS, et al. Clinical practice guideline (update): adult sinusitis. *Otolaryngol Head Neck Surg*. 2015;152(2 Suppl):S1–S39. doi:10.1177/0194599815572097

10. Kyriakis JM, Avruch J. Mammalian MAPK signal transduction pathways activated by stress and inflammation: a 10-year update. *Physiol Rev*. 2012;92(2):689–737. doi:10.1152/physrev.00028.2011
11. Arthur JSC, Ley SC. Mitogen-activated protein kinases in innate immunity. *Nat Rev Immunol*. 2013;13(9):679–692. doi:10.1038/nri3495
12. Daina A, Michielin O, Zoete V. SwissTargetPrediction: updated data and new features for efficient prediction of protein targets of small molecules. *Nucleic Acids Res*. 2019;47(W1):W357–W364. doi:10.1093/nar/gkz382
13. Kim S. Getting the most out of PubChem for virtual screening. *Expert Opin Drug Discov*. 2016;11(9):843–855. doi:10.1080/17460441.2016.1216967
14. Ji Y, Liu Y, Hu J, et al. Exploring the molecular mechanism of *Astragali Radix-Curcumae Rhizoma* against gastric intraepithelial neoplasia by network pharmacology and molecular docking. *Evid Based Complement Alternat Med*. 2021;2021:8578615. doi:10.1155/2021/8578615
15. Wang YJ, Chen S, Chen JJ, et al. Bacterial biofilm formation after nasal packing in nasal mucosa-wounded mice. *Am J Rhinol Allergy*. 2013;27(4):e91–e95. doi:10.2500/ajra.2013.27.3938
16. Liu XZ, Zheng RX, Liu Q. Protective effects of Xin'an Biyuan Fang extracts against acute sinusitis in rats [in Chinese]. *J Anhui Univ Chin Med*. 2012;31(2):48–52.
17. Akanda MR, Kim IS, Ahn D, et al. Anti-inflammatory and gastroprotective roles of Rabdosia inflexa through downregulation of pro-inflammatory cytokines and MAPK/NF-κB signaling pathways. *Int J Mol Sci*. 2018;19(2):482. doi:10.3390/ijms19020482
18. Ma Y, Tian P, Zhong H, et al. WDPCP modulates cilia beating through the MAPK/ERK pathway in chronic rhinosinusitis with nasal polyps. *Front Cell Dev Biol*. 2021;9:630340. doi:10.3389/fcell.2020.630340
19. Wang H, Lu X, Cao PP, et al. Histological and immunological observations of bacterial and allergic chronic rhinosinusitis in the mouse. *Am J Rhinol*. 2008;22(4):343–348. doi:10.2500/ajr.2008.22.3184
20. Jin MZ, Gu ZW, Bian ZG, et al. Developing a mouse model of acute bacterial rhinosinusitis. *Eur Arch Otorhinolaryngol*. 2011;268(6):857–861. doi:10.1007/s00405-011-1483-4
21. Liang X, Shen Y, Zhang XW, He GX, Tan GL. Ethyl pyruvate ameliorates inflammatory response of sinonasal mucosa by inhibiting HMGB1 in rats with acute rhinosinusitis. *Sci Rep*. 2021;11(1):7331. doi:10.1038/s41598-021-85785-3
22. Chegini Z, Noei M, Hemmati J, Arabestani MR, Shariati A. The destruction of mucosal barriers, epithelial remodeling, and impaired mucociliary clearance: possible pathogenic mechanisms of *Pseudomonas aeruginosa* and *Staphylococcus aureus* in chronic rhinosinusitis. *Cell Commun Signal*. 2023;21(1):87. doi:10.1186/s12964-023-01347-2
23. Cloonan SM, Glass K, Laucho-Contreras ME, et al. Mitochondrial iron chelation ameliorates cigarette smoke-induced bronchitis and emphysema in mice. *Nat Med*. 2016;22(2):163–174. doi:10.1038/nm.4021
24. Liu G, Summer R. Cellular metabolism in lung health and disease. *Annu Rev Physiol*. 2019;81(1):403–428. doi:10.1146/annurev-physiol-020518-114640
25. England RJ, Homer JJ, Knight LC, Ell SR. Nasal pH measurement: a reliable and repeatable parameter. *Clin Otolaryngol Allied Sci*. 1999;24(1):67–68. doi:10.1046/j.1365-2273.1999.00223.x
26. Singh V, Kaur R, Kumari P, Pasricha C, Singh R. ICAM-1 and VCAM-1: gatekeepers in various inflammatory and cardiovascular disorders. *Clin Chim Acta*. 2023;548:117487. doi:10.1016/j.cca.2023.117487
27. Tingsgaard PK, Bock T, Lange Vejlsgaard G, Tos M. Expression of intercellular adhesion molecule-1 on the vascular endothelium in nasal polyps before, during and after topical glucocorticoid treatment. *Acta Otolaryngol*. 1998;118(3):404–408. doi:10.1080/00016489850183511
28. Yao XL, Wang SB, Chen YC, et al. Sodium houttuyfonate attenuates neurological defects after traumatic brain injury in mice via inhibiting NLRP3 inflammasomes. *J Biochem Mol Toxicol*. 2021;35(9):e22850. doi:10.1002/jbt.22850